Extreme Mechanics Letters 21 (2018) 35–43

Contents lists available at ScienceDirect

Extreme Mechanics Letters

journal homepage: www.elsevier.com/locate/eml

Stimuli-induced bi-directional hydrogel unimorph actuators

Shanliangzi Liu [a,b], Elisa Boatti [c], Katia Bertoldi [c,d], Rebecca Kramer-Bottiglio [a,b,*]

[a] School of Mechanical Engineering, Purdue University, West Lafayette, IN 47907, USA
[b] Department of Mechanical Engineering and Materials Science, Yale University, New Haven, CT 06511, USA
[c] John A. Paulson School of Engineering and Applied Sciences, Harvard University, Cambridge, MA 02138, USA
[d] Kavli Institute, Harvard University, Cambridge, MA 02138, USA

ARTICLE INFO

Article history:
Received 26 January 2018
Received in revised form 14 March 2018
Accepted 14 March 2018
Available online 22 March 2018

Keywords:
Hydrogel-elastomer
Humidity-sensitive
Interfacial bond
Bi-directional

ABSTRACT

Stimuli responsive hydrogels may be promising materials for shape transforming structures due to their ability to deform significantly in response to an environmental stimulus without the need for external power. It is well-known that by laminating swelling hydrogels and non-swelling flexible materials, such as inert elastomers, bending actuation can be achieved. In this work, we report an improved hydrogel-elastomer bonding process and demonstrate the utility of the process with a stimuli-induced bi-directional hydrogel unimorph actuator. The actuator is comprised of polyacrylamide (PAAm) hydrogel, a humidity-sensitive gel that can swell to 17 times its original volume, bonded to polydimethylsiloxane (PDMS) elastomer, which is humidity insensitive. The unimorph actuator bends in one direction during swelling in an aqueous environment and in the opposite direction when drying in air, without any observed delamination between layers. We achieve the strong bonding between PAAm hydrogel and PDMS elastomer through both chemical and mechanical means, and quantify an order-of-magnitude improvement in interfacial bond strength relative to bonding through chemical means alone. We observe the bi-directional bending behavior of hydrogel unimorph actuators as a function of environmental humidity and prove that the structure's motion can be tuned by manipulating the thickness of the PDMS elastomer layer, as well as predicted using a simplified analytical approach. Lastly, we expand upon a simple rectangular unimorph structure to demonstrate more complex bending, wrinkling, and surface texture behaviors.

1. Introduction

Soft, intricate multifunctional structures seen in nature [1–4] have inspired the design of shape transforming materials capable of reconfiguration in response to environmental stimuli [5]. Various kinds of materials have been shown to exhibit shape changing behaviors, including shape memory alloys [6,7], electroactive polymers [8–10], shape memory polymers [11,12] and polymer gels [13,14]. Such materials have applications in microfluidics [15–17], biomedical devices [18–20], soft robotics [21–23], optical devices [24,25], microfabrication [26–28] and stimuli-responsive surfaces [29–31]. As a class of stimuli-responsive materials, hydrogels are able to change volume with reversible swelling and deswelling in response to environmental stimuli such as temperature [32–39], pH [32,40–43], light [44–46], enzymes [47], ion strength and solvent composition [48,49], electric and magnetic fields [14,21,50,51], elastic instabilities and surface oscillation [52,53]. The earliest published results on hydrogel actuation used the material for liquid flow control in microfluidic devices [17,38,39,54,55]. In these systems, hydrogels served as valves and underwent homogeneous expansion and shrinkage to control fluid flow. However, homogeneous swelling and deswelling only result in volumetric material changes. Shape change induced by inhomogeneous deformations, such as bending [11,21,34,49,56], twisting [11,49,56] and buckling [57,58] require more complex designs of hydrogel composites. A number of approaches have been developed to make reversible and controllable 3D shape-changing systems by integrating multiple active layers with different soft material networks that respond differently to the same stimulus. For instance, electro-actuated hydrogel walkers have been achieved by incorporating two opposite charge hydrogels: acrylamide (AAm)/sodium acrylate (NaAc) copolymer and acrylamide/quaternized dimethylaminoethyl methacrylate (DMAEM A-Q) copolymer that deform in opposite directions in response to electric fields in aqueous solutions [21]. Also, 3D printed reversible shape changing components have been demonstrated by integrating hydrogels with shape memory polymers (SMPs), which are regulated by both the swelling properties of hydrogels and the temperature sensitivities of SMPs [11].

* Corresponding author.
E-mail address: rebecca.kramer@yale.edu (R. Kramer-Bottiglio).

https://doi.org/10.1016/j.eml.2018.03.001
2352-4316/

Several studies have focused on aqueous-induced bi-directional reversible 3D shape changing structures by integrating hydrogels with other soft materials [11,21,42,56,59–61]. In these previous works, the interfacial bond strength between active and inactive materials has often not been evaluated, with only a few observable cycles reported [36,42]. Soft material systems that can attain many cycles of bidirectional bending triggered by swelling and deswelling with controllable interfacial strength and structures have yet to be achieved. Such systems could be embedded into soft mechanical assemblies and enable functionality in an ordinary aqueous environment with only a single stimulus.

In this work, we describe a humidity-sensitive bi-directional hydrogel unimorph actuator enabled by coupled chemical and mechanical interfacial bond processes. The bending actuator is comprised of an active hydrogel layer (polyacrylamide (PAAm)) and an inactive elastomer layer (Sylgard 184 polydimethylsiloxane (PDMS)), where the interfacial bond strength between the two materials is controllable by the adjusting contact area via surface texture of the elastomer.

Leveraging the high swelling ratio of polyacrylamide hydrogel, we achieve large shape changes using differential swelling in the unimorph structure without any delamination between layers. We further analytically predict the curvature of rectangular bi-layered unimorph structures as a function of elastomer layer thicknesses. Finally, we extend the robust bonding technique to more complex structures to demonstrate a blooming and un-blooming soft flower, as well as changes in surface wrinkling and surface texture induced by humidity.

2. Results and discussion

2.1. Hydrogel unimorph actuator fabrication

Tough bonding between a hydrogel and an elastomer is required to achieve remarkable bending behavior using hydrogels with high swelling ratios. We selected acrylamide as the monomer to form polyacrylamide hydrogel with a swelling ratio of ∼17 when fully swollen. The swelling ratio of polyacrylamide hydrogel as a function of time is shown in Figure S1 (Supporting Information). A schematic of the hydrogel unimorph actuator fabrication process is shown in Fig. 1. First, the surface of an acrylic mold was textured using a laser engraving system (Universal Laser Systems VLS 2.30, fitted with a 30 W CO_2 laser). The laser engraved lines in perpendicular directions on the surface, which resulted in micro-scale texture (Fig. 1(a)–(b)). We note here that surface texture can be easily tuned using this approach by adjusting power and speed of the laser, as detailed in the Experimental Section. Next, a micro-textured PDMS elastomer sheet was made by pouring liquid elastomer after mixing and defoaming into the laser-textured acrylic mold, followed by a degassing step in air for an hour to remove extra air bubbles and a cure step at 60 °C for 1.5 h (Fig. 1(c)). Once cured, the elastomer was removed from the mold and flipped (Fig. 1(d)). Then, the micro-textured PDMS elastomer surface was modified by exposure to oxygen plasma to produce hydroxyl groups on the surface. Exposed surface hydroxyl groups enabled grafting of 3-(Trimethoxysilyl)propyl methacrylate (TMSPMA), which generated methacrylate groups on the surface and served as a chemical adhesive in the subsequent step (Fig. 1(e)). Next, PAAm pre-gel solution was poured into a smooth acrylic mold and the TMSPMA-functionalized micro-textured PDMS elastomer was placed over the solution (Fig. 1(f)). The exposed methacrylate groups on the PDMS elastomer surface formed linkage with acrylate groups in acrylamide under UV photo-polymerization (Fig. 1(g)), generating PAAm hydrogel chemically bonded onto PDMS elastomer. Finally, after fabrication of the bilayer sheet, hydrogel unimorph actuators (30 mm × 4 mm) were cut using the laser engraving system (Fig. 1(h)). We note here that a variety of tools and methods may be used to define the cut shape of the unimorph, and that more intricate 2D shapes would result in more complex 3D structures upon swelling and deswelling.

2.2. Hydrogel-elastomer interfacial bond strength

The primary novelty of the enhanced hydrogel-elastomer bonding process is the introduction of continuous texture to the bonded surfaces, which increases the area of interaction between those surfaces (Fig. 2(a)). Our approach was inspired by Zhang et al. [62], who employed micro-pillar surface structures fabricated using photolithography to enhance bonding. Here, we employ a continuous surface texture produced by laser rastering to further reduce the hydrophobicity of the surface (relative to a non-continuous texture) while maintaining increased contact area. Texture created by laser rastering is also a highly scalable, fast and easy process.

We evaluated the strength of the interfacial bond between the elastomer and the hydrogel in the flat state (right after UV curing). To measure the interfacial bond strength of hydrogel-elastomer bonding, 90° peel strength tests were performed using an Instron materials testing system. As illustrated in Fig. 2(b), a stiff polyethylene terephthalate (PET) film was attached to the top surface of the hydrogel with cyanoacrylate to avoid hydrogel stretching during peeling. The bottom surface of the elastomer was adhered to a 3D printed adapter fixed to the Instron using elastomer as the adhesive. The adhesive elastomer was poured into trapezoidal channels in the adapter plate and the cured hydrogel-elastomer bilayer was placed on top. When cured, this provides a strong mechanical bond to the adapter plate below, and a strong chemical bond to the elastomer layer above. The samples were sealed in a pan filled with water until taken out for peel tests to prevent drying. We determined that dehydration over the duration of the tests was negligible since the tests only required a few minutes. The dehydration ratio is plotted as a function of dehydration time as shown in Figure S2 (Supporting Information). All the peel tests were performed with a constant peeling rate of 20 mm/min. The interfacial bond strength is calculated as the peeling force in the steady state per unit width and measured in units of N/m [63–65].

To measure the effect of surface texturing, we evaluated hydro gel-elastomer interfacial bond strength as a function of surface roughness. Different surface roughnesses were achieved by adjusting the laser power and speed settings. We analyzed the laser-textured surface using an optical profiler (Zeta Instruments) and measured the root mean square roughness (S_{rms}; root mean square average of the roughness data points) and surface area ratio (S_{dr}; the actual interfacial surface area relative to the geometric projected surface area). As shown in Fig. 2(c), the interfacial bond strength initially improves with increasing surface roughness due to increasing contact area at the material interface. At a surface roughness of $S_{rms} = 28.85\ \mu m$ $S_{dr} = 2.30$, the bond strength peaks (∼500 N/m) and monotonically decreases with increasing surface roughness thereafter. We attribute this to wetting mechanics between the liquid hydrogel solution and the rough elastomer surface. As surface roughness initially increases, wetting is characterized as a Wenzel state, where homogeneous wetting means that increasing the elastomer surface roughness increases the contact area between the liquid hydrogel and elastomer. However, above a critical surface roughness threshold, wetting is characterized as a Cassie state, where the liquid cannot fully penetrate the roughness and contact area at the liquid–solid interface decreases. In our experiments, this decreasing contact area manifests as decreasing interfacial bond strength, and the peak indicated in Fig. 2(c) marks the Wenzel–Cassie transition where interfacial bond strength is optimized.

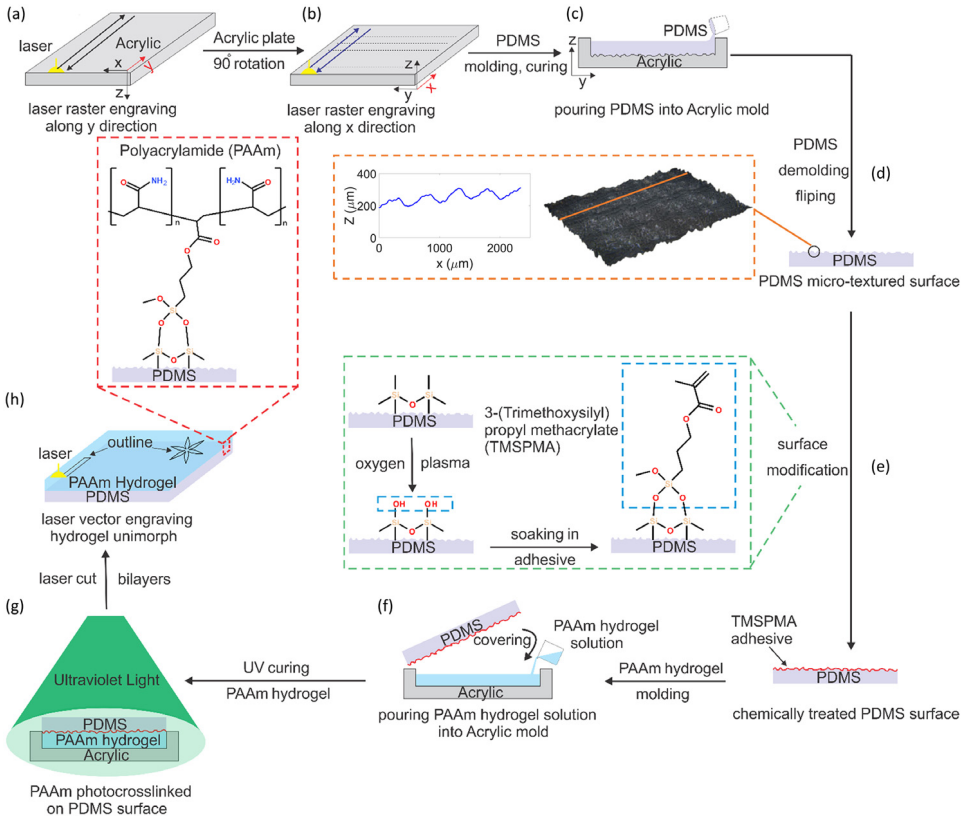

Fig. 1. Schematic of hydrogel unimorph actuators fabrication process. (a) Laser engraving on acrylic sheet along *y* direction. (b) Rotating the acrylic sheet by 90° to engrave along *x* direction. (c) Pouring uncured PDMS into laser-textured acrylic mold. (d) Peeling the cured PDMS from the mold and flipping. The inset shows 3D image of the micro-textured PDMS surface and a z profile of the line section. (e) Chemically modifying micro-textured PDMS surface (oxygen plasma followed by 3-(Trimethoxysilyl)propyl methacrylate (TMSPMA) grafting). (f) Pouring the pre-gel solution onto the micro-textured, chemically treated PDMS and then (g) photo-polymerizing under UV. (h) Laser cutting unimorph actuators from the bilayer. The inset shows the exposed methacrylate groups on the PDMS surface formed linkage with acrylate groups in acrylamide.

Using the optimized surface roughness parameters, we measured the contact angle between water and the chemically unmodified laser-textured elastomer surface to be approximately 121.6°, and the same static contact angle using our PAAm hydrogel solution in place of water was measured as approximately 110.5°. Furthermore, this contact angle reduces to approximately 25° after chemical surface modification, which indicates strong wetting of the hydrogel to the elastomer surface, resulting in increased bonding sites and a stronger interfacial bond. The dramatic reduction in contact angle in response to chemical surface modification highlights the importance of the chemical contribution to the overall bonding process.

Hydrogel was also bonded to non-textured elastomer using the same chemical treatment as the micro-textured elastomer surfaces. Without surface texturing, the hydrogel layer was easily peeled off the PDMS with no surface deformations observed (Fig. 2(d)). In contrast, as shown in Fig. 2(e), hydrogel peeling from the micro-textured elastomer surface occurred in two phases. First, stretching at the interface was observed as the stress on the hydrogel layer was increased. Second, once the critical tear force was reached, mechanical failure initiated at the edge of the hydrogel and propagated down the length of the film. We further note that after the peel tests, hydrogel remnants remained on the PDMS surfaces for all the samples, which indicates that the hydrogel-elastomer bond strength exceeds the tensile strength of the hydrogel.

Representative data from the peel tests are shown in Fig. 2(f). The interfacial bond strength between chemically modified (non-textured) elastomer surfaces and hydrogel is found to be ∼14 N/m. As a comparison, Yuk et al. assembled polyacrylamide common hydrogels and elastomers into hybrids by modifying elastomer surfaces with benzophenone [63]. The measured interfacial bond strength between the non-textured elastomer (chemically treated) and the polyacrylamide hydrogel layer achieved here is comparable to their results (∼25 N/m), which indicates that the surface treatment we use is on-par with state-of-the-art techniques. By creating surface microtextures, the value is increased by an order-of-magnitude (∼500 N/m).

Since the bilayer structures are to be actuated in an aqueous environment, cyclic testing was conducted to determine if the bonding between the two materials is sufficient to resist the deformation of the hydrogel layer caused by water intake. As illustrated in Fig. 2(g), one end of the unimorph was fixed onto a 3D printed stage. The unimorph then went through cycles of hydration and dehydration with different color-coded water representing different cycles. As of this writing, samples have undergone more than 50 swelling–deswelling cycles without any delamination observed. When unwanted external forces were applied during operation, the textured actuators remained operative, as observed from the unimorph samples of other shapes shown in Figure S3 (Supporting Information). No delamination occurred during bending, squeezing, twisting or stretching as shown in Video S1 (Supporting Information).

2.3. Quantifying curvature of hydrogel unimorph actuator

We sought to show that unimorph actuation may be manipulated by tuning the thickness of the elastomer layer. The hydrogel-elastomer bilayer strips (30 mm × 4 mm) were cut by laser from a large bilayer sheet and fully dehydrated in an incubator at 60 °C. Next, with one end fixed, the unimorph strips were immersed in a water bath and observed as a function of time. Hydrogel hydration

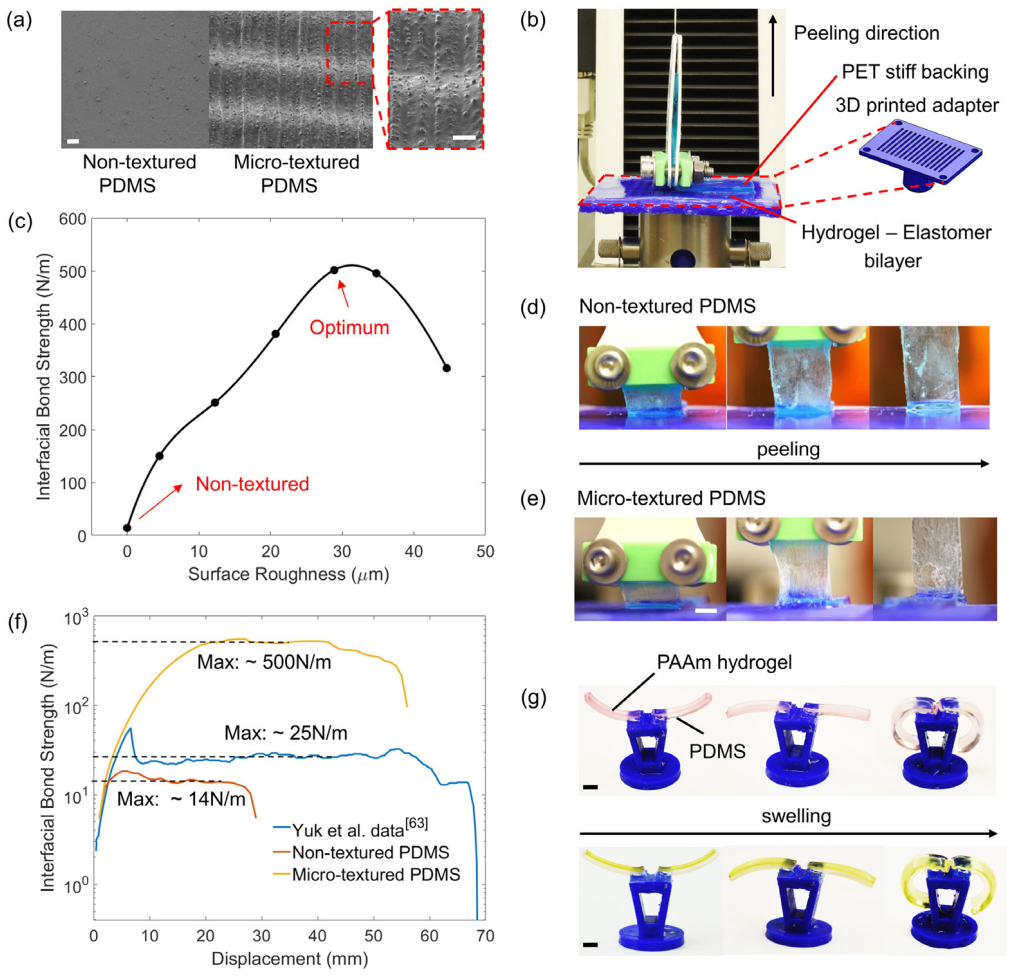

Fig. 2. Experimental results of peel strength tests, surface roughness optimization and cyclic tests. (a) SEM images of non-textured and micro-textured PDMS surfaces. The scale bars represent 100 μm. (b) Experimental setup for peel strength tests. (c) Plot of interfacial bond strength versus surface roughness of elastomer surfaces. (d) Peeling process of PAAm hydrogel bonded on non-textured, chemical treated PDMS in the flat state. (e) Peeling process of PAAm hydrogel bonded on micro-textured, chemical treated PDMS in the flat state (right after UV curing). (f) Plot of measured interfacial bond strength versus displacement for PAAm hydrogel bonded on chemically treated non-textured and micro-textured PDMS, and a referenced result from published work [63]. The *y* axis is in logarithmic scale. (g) Hydrogel unimorph actuators in fully dried, half-way dried and fully swollen states. The scale bars represent 7.5 mm.

during the experiment setup was assumed to be negligible since the air exposure time was minimized (a few minutes). We tested two groups of samples, both with a hydrogel layer thickness of ∼200 μm in the flat state (right after UV curing), but differing in PDMS layer thickness. We denote a "thick actuator" group with a PDMS layer thickness of ∼1000 μm and a "thin actuator" group with a PDMS thickness of ∼600 μm Fig. 3(a)–(b) shows representative thin and thick unimorph actuators swelling in an aqueous environment over 30 min and 7 h, respectively. The PDMS layers are in pink color, and the PAAm layers are transparent. The curvature changes over time of the two samples are shown in Video S2 (Supporting Information). The thin actuator (Fig. 3(a)) and the thick actuator (Fig. 3(b)) have similar initial bending curvature and comparable shape configurations, and they reach the same position when they are fully actuated. However, the actuation time for the thin actuator is 13 times less than the thick actuator.

The bending behavior of the hydrogel unimorph actuators sh own in Fig. 3(a)–(b) is attributed to inhomogeneous 1D constrained swelling of the hydrogel layer in water. There are two primary effects which cause this behavior. First, the stress state within the hydrogel is different along the thickness direction. When stressed, the hydrogel cannot absorb additional water, hence swelling is constrained near the interface between the hydrogel and elastomer layers. Second, water absorption is limited by diffusion through the hydrogel. Thus, water must be absorbed first by the exposed hydrogel surface, then diffuse through the hydrogel layer to the inner material. After swelling is complete, the hydrogel layer has compressive stress at the interface, and tensile stress at the surface. When in the dehydrated state, the reverse is true. Physically, this manifests as the bilayer strip bending towards the inextensible elastomer layer in the swollen state and the opposite direction in the dehydrated state. The bilayer material with thicker elastomer is stiffer, thus requiring more stress and swelling time to achieve the same curvature. Additionally, the stress generated by the swelling of the hydrogel is biaxial. In order to constrain the bending to a single direction, the aspect ratio of laser-cut parts is set to 7.5 (30 mm × 4 mm), which causes the bending in the long axis to dominate bending in the short axis.

To further analyze the bending behavior of the unimorph actuators, the bending curvature of the hydrogel-elastomer bilayers corresponding to the samples in Fig. 3(a)–(b) is plotted as a function of time as shown in Fig. 3(c)–(d). Both the thick and thin actuator exhibit a three-phase hydration sequence: (1) an increase in curvature in the direction of the dehydrated state, (2) an abrupt transition and reversal of the curvature, and (3) increasing curvature in the direction of the hydrated state. We initially hypothesized two reasons for the initial curvature change in the direction of dehydrated state: water diffusion into PDMS elastomer

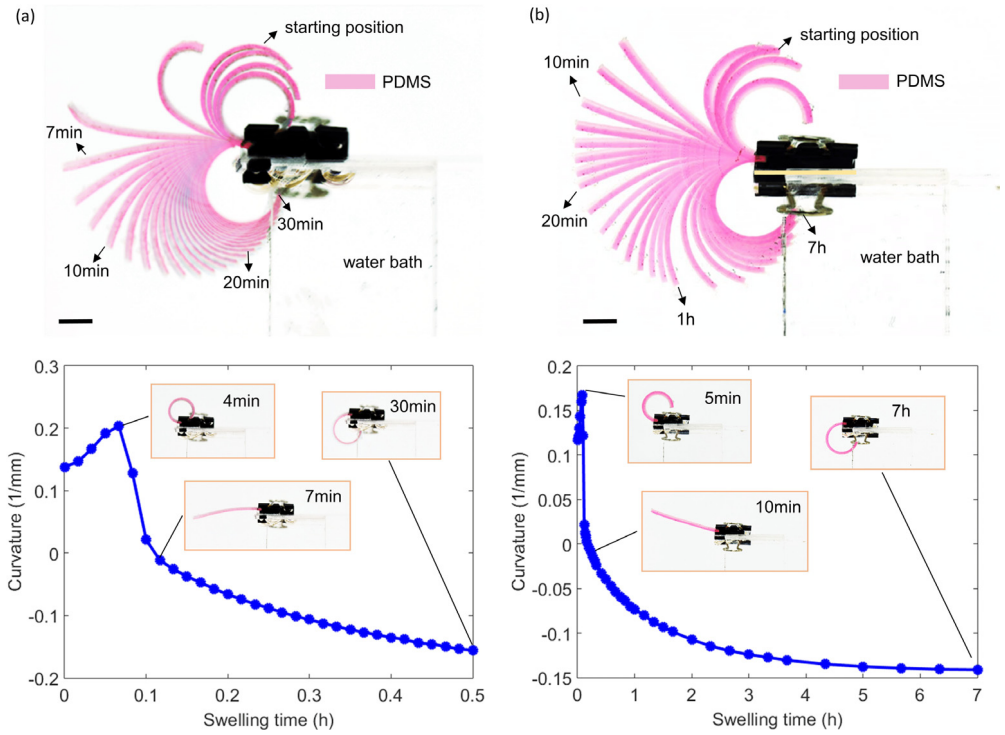

Fig. 3. Bending behavior of unimorph actuators in aqueous environment. (a) Overlaid photo sequence of the thin actuator curvature change over a duration of 30 min. (b) Overlaid photo sequence of the thick actuator curvature change over a duration of 7 h. The scale bars represent 5 mm. (c) Experimentally measured bending curvature of the thin actuator corresponding to (a). (d) Experimentally measured bending curvature of the thick actuator corresponding to (b).

and thermal effects. According to Lee et al. [66] and as well as our own simple experiments (detailed in the Experimental Section), PDMS elastomer is not able to absorb enough water to increase the bending curvature at first. A more reasonable explanation is thermal contraction of the hydrogel. During the curvature tests, the unimorph was immersed in 20 °C water only minutes after removal from an incubator at 60 °C, which caused immediate thermal contraction. By increasing the water bath temperature to 60 °C to match the temperature of the incubator, we found that the initial curvature increase was reduced from ∼15% to ∼5%. In addition, it took only 2 s to reverse the curvature direction in the 60 °C water bath, while this reversal took 5 s in the 20 °C bath.

2.4. Hydrogel actuator bending behavior prediction

With the aim to facilitate the design of hydrogel actuators capable of achieving targeted responses, we adopted a simple strategy that allows to predict the evolution of their curvature as a function of the swelling time. Although it has been recently shown that the transient response of gels can be captured by treating the material as hyperelastic and adopting the nonlinear field theory of coupled diffusion and deformation [67–69], such simulation procedures are complex and normally require a high number of parameters and a relatively high computational effort. Therefore, we took a simplified approach that builds on the Timoshenko formula [70]. This formula was originally developed to capture the bending deformation of a uniformly heated bilayer strip with different expansion coefficients for each layer, but it has been shown that is also appropriate to describe the behavior of bilayers including a swollen soft material [71,72].

Our simplified analytical approach is based on the following assumptions: (1) negligible curvature along the width of the sample, (2) uniform, isotropic and linear elastic material properties, and (3) negligible solvent diffusion and uniform swelling throughout the hydrogel layer at each time instant. Importantly, our approach does not require a *priori* knowledge of material parameters other than the Young's moduli of the two layers and can predict with a satisfactory degree of accuracy the motion of unimorphs with identical PAAm thickness, but different PDMS thicknesses, by using the data extracted from a single experiment.

We started by using one experimental test to determine the evolution of the swelling strain of the hydrogel layer as shown in Fig. 4(a). The swelling strain was easily inferred from the experimentally obtained curvature-time relationship, by using for each time instant the Timoshenko formula,

$$\varepsilon_{PAAm}(t) = -\frac{\kappa(t)\cdot h(3(1+m)^2+(1+m\cdot n)(m^2+\frac{1}{m\cdot n}))}{6(1+m)^2} \quad (1)$$

where is $\varepsilon_{\mathrm{PAAm}}(t)$ is the swelling strain for the hydrogel layer at time t, which is assumed to be constant in the material [73], $\kappa(t)$ is the experimentally measured curvature at time t, $m = h_{\mathrm{PDMS}}/h_{\mathrm{PAAm}}$ is the ratio of the thickness of the two layers in the flat state, $n = E_{\mathrm{PDMS}}/E_{\mathrm{PAAm}}$ is the ratio of the Young's moduli of the two materials that are shown in Figure S4 (Supporting Information) and $h = h_{\mathrm{PDMS}} + h_{\mathrm{PAAm}}$ is the total thickness of the unimorph. In Eq. (1), we assumed that $\varepsilon_{\mathrm{PDMS}} = 0$, since PDMS elastomer does not swell in water. In Fig. 4(a) we report the evolution of the swelling strain obtained for a sample characterized by and $h_{\mathrm{PDMS}} = 1000\ \mu\mathrm{m}$ and $h_{\mathrm{PAAm}} = 200\ \mu\mathrm{m}$. In this analysis, we considered only the swelling process that starts when the experimentally measured curvature begins to decrease and we assumed that at $\Delta t = 0$ the sample is fully dried.

Next, we used the obtained swelling strain curve and Eq. (1) to predict the curvature evolution for other samples characterized by h_{PAAm}, but different values of h_{PDMS}. In Fig. 4(b) we report the analytically predicted evolutions of the curvature during swelling for a range of h_{PDMS}, while holding $h_{\mathrm{PAAm}} = 200\ \mu\mathrm{m}$ constant. Despite the simplicity of the approach, for $h_{\mathrm{PDMS}} = 600\ \mu\mathrm{m}$ agreement is found between analytical and numerical results as seen from the unimorph configurations in Fig. 4(c), suggesting

that the approach can be used to design unimorphs with desired responses. However, it should be noted that in the initial minutes when dynamic swelling is faster, the curvature is more difficult to capture and predict, thus the experimental and analytical results do not perfectly overlap. Finally, since the thickness of the hydrogel layer affects its swelling rate, we note that our approach requires recalculation of a new swelling evolution curve from experimental data for each different thickness value of the hydrogel layer. Additional experimental and analytical results for the unimorph samples are included in Figure S5–6 (Supporting Information).

2.5. 3D shape changing objects

To prove that hydrogel deformations induced by swelling constrained on an elastomer surface can lead to significant shape change in two directions, and that the bond strength on the interface is strong enough to resist the large deformations, we sought to demonstrate various 3D shape changing structures including a blooming and un-blooming soft flower, as well as changes in surface wrinkling and surface texture induced by humidity.

As observed previously, the bilayer structures of different thickness have different rates of curvature change. To illustrate this point, we fabricated a single flower structure composed of a thinner unimorph forming the top inner petals and a thicker unimorph forming the bottom outer petals, as shown in Fig. 5(a). This results in fast reactions of the top petals while swelling/deswelling, as well as larger curvature change when compared to the bottom petals. The flower structure was designed in a 2D graphic tool and cut directly from the bilayer sheets by a laser cutter. The top petals were attached to the bottom petals when both were fully dried and curved towards the hydrogel side, as illustrated in Fig. 5(a). To highlight the two layers, the elastomer layer of the top petals were dyed green and the bottom petals were dyed orange. When immersed in blue coded water for ∼10 min, both hydrogel layers swell, forming a blooming flower in the opposite direction of the dried state. After removing the flower from the water bath, the structure starts to dry, and the bending curvature is reduced. Eventually, it recovers to the fully dried state.

We further sought to show that the strong hydrogel-elastomer bond could also be applied to stimuli-responsive surfaces in soft systems. If the elastomer layer of the unimorph structure is thick enough relative to the hydrogel layer, the stress generated during hydrogel swelling is not large enough to cause any curvature change. This is demonstrated in Fig. 5(c) where shapes such as the hydrogel letters "FAB" and pillars are bonded onto elastomer substrates. After immersion in water, the hydrogel layer swells, with the elastomer as a stiff supporting substrate. In Fig. 5(b), swelling of the high aspect ratio letters that are bonded to the elastomer induces wrinkling, and the shape recovers when fully dried. In Fig. 5(c), swelling of the pillars changes the surface texture. The swollen hydrogel pillars are inverse-trapezoidal due to constrained swelling at the bottom, while the top swells freely in all directions allowing neighboring pillars to connect. When fully dried, the pillars are separated again. Optical images of a hydrogel pillar in dried and swollen states and thickness profiles of the line sections are shown in Figure S7 (Supporting Information). In both Fig. 5(b) and (c), dye molecules are left within the hydrogel matrix after immersion in color-coded water. Upon re-swelling, these dye molecules dissipate and take on the color of the new aqueous medium.

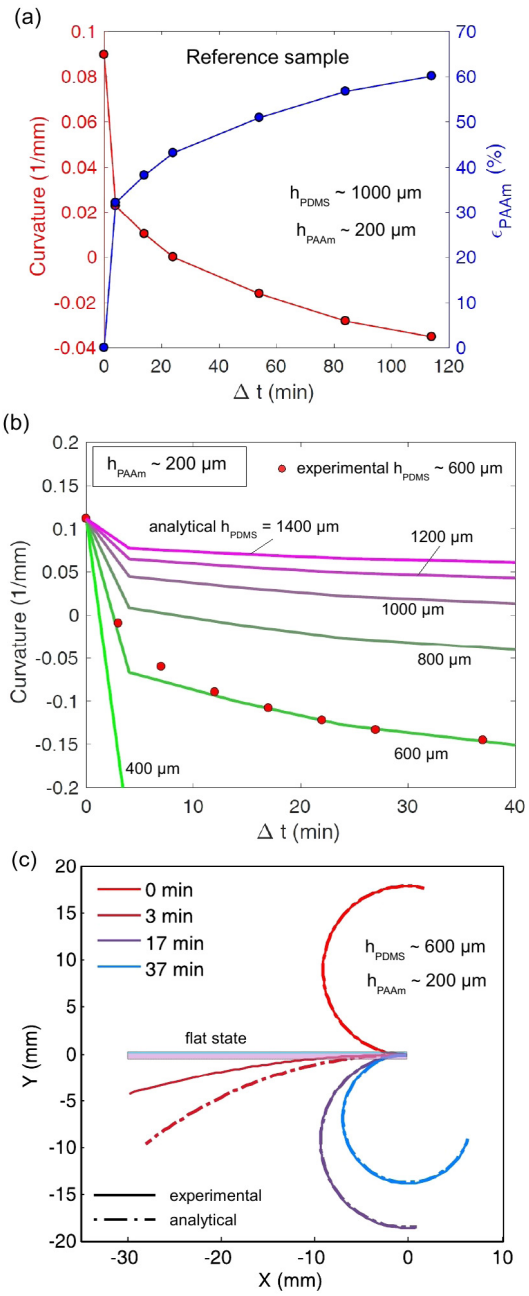

Fig. 4. Comparison between experimental and analytical results for hydrogel unimorph actuator. (a) Curvature evolution for the reference sample (h_{PDMS} = 1000 μm and h_{PAAm} = 200 μm) and corresponding swelling strain evolution of the PAAm hydrogel layer ε_{PAAm} obtained using Eq. (1). (b) Predicted curvature evolutions for different PDMS elastomer thicknesses (assuming h_{PAAm} = 200 μm); experimental data for the case h_{PDMS} = 600 μm are reported as markers. (c) Comparison between experimentally observed and analytically predicted configurations for a bistrip with h_{PDMS} = 600 μm and h_{PAAm} = 200 μm at different time instants.

3. Conclusion

In this work, we have demonstrated a stimuli-induced bi-directional hydrogel unimorph actuator that can swell and deform in aqueous environments without the need for any additional stimulus and deform in the opposite direction when fully dried. To achieve this, we have bonded a large swelling ratio PAAm hydrogel onto a PDMS elastomer using both chemical modification and continuous micro-textures. We have quantified an order-of-magnitude improvement in interfacial bond strength relative to bonding through chemical means alone. Furthermore, we have demonstrated that the bending behavior of the actuator can be tuned by the relative thickness of the two layers and successfully predicted by a simplified analytical approach. We also have shown

Fig. 5. Illustration of bilayer 3D shape changing objects. (a) Blooming flower 2D pattern and 3D object when fully dried, fully swollen and half-way dried. (b)–(c) PAAm hydrogel letters and pillars bonded on PDMS substrates, and the surface texturing and wrinkling induced by humidity. The scale bars represent 4 mm.

that this fabrication process can produce more complex 3D reversible shape transforming structures operated in aqueous environments. The proposed fabrication techniques may be extended to other types of polymers and used to achieve 3D shapes towards developing more complex bidirectional structures and stimuli responsive surfaces. Further optimization of the analytical approach will enable the prediction of more complex shape transforming behaviors.

4. Experimental

4.1. Materials

Acrylamide (AAm; Sigma–Aldrich A8887; $\geq$ 99%), 2-Hydroxy-2-methylpropioph-enone (Irgacure 1173; Sigma–Aldrich 405655; 97%), N, N'-Methylenebisacrylamide (MBAM; Sigma–Aldrich M7 279; $\geq$ 99.5%), Polydimethylsiloxane (PDMS Elastomer; Dow Corning Sylgard 184 Silicone Elastomer Kit). PDMS elastomers were colored by mixing with silicone color pigments (Silc Pig; Smooth-On). Hydrogel solutions were dyed with food color (Electric Color Soft Gel Paste Food Color 12 Pack Kit; Americolor). PET films (thickness 0.025 mm; McMaster–Carr; 8567K12) were used as a stiff backing on the top surface of the hydrogel layer during the 90° peel strength tests, together with cyanoacrylate (Loctite Instant-Bonding Adhesive 414; McMaster–Carr; 7625A16) as the adhesive. Both PDMS elastomers and PAAm hydrogels were molded from optically clear acrylic sheets (thickness 2 mm, 3.175 mm, McMaster–Carr), and 3D printed PLA frames (thickness 1 mm, 0.6 mm, McMaster–Carr) were used as the spacers for the acrylic molds.

4.2. Hydrogel and elastomer polymerization

PAAm Hydrogels were prepared by photo-polymerizing acrylamide monomers using MBAM as a crosslinker and Irgacure 1173 as a photoinitiator. The aqueous pre-gel solutions (65.4 wt% deionized water, 33.4 wt% acrylamide, 0.05 wt% MBAM, 1.2 wt% Irgacure 1173) were mixed, degassed and then irradiated under the 10 mW/cm^2 ultraviolet light (OAI Model 30 UV Light Source) for 80 s. PDMS elastomers were prepared by mixing the elastomer base and the curing agent in a 10:1 ratio using a Thinky Mixer (Planetary Centrifugal Solder Paste Mixer SR-500) for one minute, then mixed elastomer sat in air for an hour to degas and cured in an incubator at 60 °C for 1.5 h.

4.3. Hydrogel unimorph actuator fabrication

The elastomer layer of the unimorph structure was molded from a laser rastered acrylic mold. A piece of 3.175 mm thickness acrylic sheet was scanned by laser to ablate material from the surface using a raster-scan mode. In this mode, the laser beam scans back and forth across the surface and pulses on and off in rapid succession (35% power, 5% speed, total laser power is 30 W) as shown in Fig. 1(a). Then, the workpiece was rotated 90° and rastered again with the same laser power and speed as shown in Fig. 1(b)). The engraved lines crossing in perpendicular directions produced a micro-scale textured acrylic surface. Liquid PDMS elastomer was poured into the rastered mold, degassed, and cured in an incubator at 60 °C for 1.5 h. The elastomer layer thickness was controlled by 3D printed spacers (600 μm, 1000 μm) clamped on the acrylic molds. Next, cured elastomers were taken out of the mold, flipped, cleaned thoroughly with isopropanol, ethanol and deionized water, and completely dried with nitrogen.

An image of the micro-textured elastomer surface (2333 μm $\times$ 1750 μm) was taken from an optical profiler (Zeta Instruments) by scanning the sample over a specified z range (446 μm) as shown in Fig. 1(d) inset). A z profile of a line section taken from the image is also included in Fig. 1(d). Root mean square roughness S_{rms} and surface area ratio S_{dr} were averaged over three boxes (500 μm $\times$ 500 μm) randomly picked from the image.

Next, a 200 μm film (100 mm $\times$ 65 mm $\times$ 3.175 mm) was made by spin coating liquid PDMS elastomer on an acrylic plate at 200 rpm for 60 s. Then, trimming off a rectangular piece (80 mm $\times$ 50 mm $\times$ 200 μm) from center of the film created a 200 μm basin to be filled by PAAm hydrogel solution. Once filled, the basin and the PDMS elastomer film around it were covered by a micro-textured PDMS elastomer layer. Next, irradiating the whole assembly under ultraviolet light for 80 s produced the desired hydrogel unimorph. Afterwards, a laser cutter (Universal Laser Systems VLS2.3) was used in the vector engraving mode to cut the rectangular shapes (30 mm $\times$ 4 mm), flower petals or other shapes from the hydrogel unimorph (50% power, 20% speed).

4.4. Laser settings for surface roughness optimization

Elastomer surfaces with textures of varying roughnesses were created. The laser settings and corresponding average surface roughness parameters in Fig. 2(c) are: 1.18% power, 90% speed, $S_{\text{rms}} = 4.48$ μm; 2. 25% power, 70% speed, $S_{\text{rms}} = 12.21$ μm; 3.

35% power, 70% speed, $S_{rms} = 20.74\ \mu m$; 4. 35% power, 5% speed, $S_{rms} = 28.85\ \mu m$; 5. 25% power, 5% speed, $S_{rms} = 34.75\ \mu m$; 6. 40% power, 5% speed, $S_{rms} = 44.62\ \mu m$.

4.5. Hydrogel-elastomer interfacial bond tests

The interfacial bond strength of hydrogel-elastomer interfaces were measured using 90° peel strength tests with the Instron testing system. Hydrogel solution was filled in an acrylic mold (100 mm × 20 mm × 3.175 mm) and covered by a chemically treated PDMS elastomer with different surface roughnesses (100 mm × 65 mm × 2 mm). After UV polymerization, the elastomer layer with the hydrogel layer bonded on top was adhered to a PLA custom pull test adapter manufactured by a PrinterBot 3D printer using liquid PDMS elastomer as the adhesive. The pull test adapter was designed to be fixed on the Instron test machine. The values reported in this paper were calculated from triplicate measurements.

4.6. Hydrogel unimorph actuator curvature tests

The hydrogel unimorph strips (30 mm × 4 mm) cut from the bilayer sheets were put into the incubator at 60 °C until fully dehydrated, then removed from the incubator and clamped with one end fixed on the fixture plate. Next, the fixture plate with the hydrogel unimorph strips were immersed in 20 °C deionized water. A Nikon D5200 camera was used to shoot one image every minute. From all the collections of images, 30 representative configurations of one individual test were picked and stacked into one image using ImageJ as shown in Fig. 3(a)–(b).

To confirm that PDMS layer is insensitive to humidity hence has no effect on the initial curvature change of hydrogel unimorphs, we took several PDMS samples (3 mm × 3 mm × 3 mm, 5 mm × 5 mm × 5 mm) and immersed them into a water bath. No dimension changes were observed over a duration of a few days. To indicate the impact of thermal effects on the initial curvature increment in the unimorph curvature tests, water in the acrylic box was heated up to 60 °C in the incubator and then the box was placed on a 60 °C hotplate during the tests. Images were taken only for the first few minutes until curvature started to increase in the direction of the hydrated state.

4.7. Material properties tests

Young's moduli of PAAm hydrogel and PDMS elastomer are input parameters for the Timoshenko [70] formula. Tensile tests for both materials were completed using an Instron testing system equipped with a 10 N load cell and grips cut from polystyrene sheets. The testing samples for both materials were formed via acrylic molds into dogbone shapes (gage width 11 mm, gage length 50 mm, total width 17 mm, total length 100 mm). The crosshead speed was set at 10 mm/min for all the tests.

Acknowledgment

This material is based upon work supported by the National Science Foundation under CAREER Grant No. 1454284. Any opinions, findings, and conclusions or recommendations expressed in this material are those of the authors and do not necessarily reflect the views of the National Science Foundation.

Appendix A. Supplementary data

Supplementary material related to this article can be found online at https://doi.org/10.1016/j.eml.2018.03.001.

References

[1] D. Evangelista, S. Hotton, J. Dumais, The mechanics of explosive dispersal and self-burial in the seeds of the filaree, *Erodium cicutarium* (Geraniaceae) 214 (2011) 521–529. http://dx.doi.org/10.1242/jeb.050567.
[2] R. Stahlberg, The phytomimetic potential of three types of hydration motors that drive nastic plant movements, Mech. Mater. 41 (2009) 1162–1171. http://dx.doi.org/10.1016/j.mechmat.2009.05.003.
[3] E. Reyssat, L. Mahadevan, Hygromorphs: from pine cones to biomimetic bilayers, J. R. Soc. Interface 6 (2009) 951–957. http://dx.doi.org/10.1098/rsif.2009.0184.
[4] D. Koller, Light-driven leaf movements, Plant Cell Environ. 13 (1990) 615–632. http://dx.doi.org/10.1111/j.1365-3040.1990.tb01079.x.
[5] K. Oliver, A. Seddon, R.S. Trask, Morphing in nature and beyond: a review of natural and synthetic shape-changing materials and mechanisms 51 (2016) 10663–10689. http://dx.doi.org/10.1007/s10853-016-0295-8.
[6] J. Mohd Jani, M. Leary, A. Subic, M.A. Gibson, A review of shape memory alloy research, applications and opportunities, Mater. Des. 56 (2014) 1078–1113. http://dx.doi.org/10.1016/j.matdes.2013.11.084.
[7] H.-T. Lin, G.G. Leisk, B. Trimmer, GoQBot: a caterpillar-inspired soft-bodied rolling robot 6 (2011) 026007. http://dx.doi.org/10.1088/1748-3182/6/2/026007.
[8] J. Biggs, K. Danielmeier, J. Hitzbleck, J. Krause, T. Kridl, S. Nowak, E. Orselli, X. Quan, D. Schapeler, W. Sutherland, J. Wagner, Electroactive polymers: Developments of and perspectives for dielectric elastomers, Angew. Chem. Int. Ed. 52 (2013) 9409–9421. http://dx.doi.org/10.1002/anie.201301918.
[9] Y. Bar-Cohen, Electroactive polymers as artificial muscles: A review, J. Spacecr. Rockets 39 (2002) 822–827. http://dx.doi.org/10.2514/2.3902.
[10] R. Pelrine, R. Kornbluh, G. Kofod, High-strain actuator materials based on dielectric elastomers, Adv. Mater. 12 (2000) 1223–1225. http://dx.doi.org/10.1002/1521-4095(200008)12:16<1223::AID-ADMA1223>3.0.CO;2-2.
[11] Y. Mao, Z. Ding, C. Yuan, S. Ai, M. Isakov, J. Wu, T. Wang, M.L. Dunn, H.J. Qi, 3D printed reversible shape changing components with stimuli responsive materials, Sci. Rep. 6 (2016) 24761. http://dx.doi.org/10.1038/srep24761.
[12] H. Meng, G. Li, A review of stimuli-responsive shape memory polymer composites, Polymer 54 (2013) 2199–2221. http://dx.doi.org/10.1016/j.polymer.2013.02.023.
[13] Y. Osada, J.-P. Gong, Soft and wet materials: Polymer gels, Adv. Mater. 10 (1998) 827–837. http://dx.doi.org/10.1002/(SICI)1521-4095(199808)10:11<827::AID-ADMA827>3.0.CO;2-L.
[14] Y. Osada, H. Okuzaki, H. Hori, A polymer gel with electrically driven motility, Nature 355 (1992) 242–244. http://dx.doi.org/10.1038/355242a0.
[15] M. Jamal, A.M. Zarafshar, D.H. Gracias, Differentially photo-crosslinked polymers enable self-assembling microfluidics, Nature Commun. 2 (2011) 527. http://dx.doi.org/10.1038/ncomms1531.
[16] L. Dong, H. Jiang, Autonomous microfluidics with stimuli-responsive hydrogels, Soft Matter. 3 (2007) 1223. http://dx.doi.org/10.1039/b706563a.
[17] Q. Yu, J.M. Bauer, J.S. Moore, D.J. Beebe, Responsive biomimetic hydrogel valve for microfluidics, Appl. Phys. Lett. 78 (2001) 2589. http://dx.doi.org/10.1063/1.1367010.
[18] K. Deligkaris, T.S. Tadele, W. Olthuis, A. van den Berg, Hydrogel-based devices for biomedical applications, Sensors Actuators B 147 (2010) 765–774. http://dx.doi.org/10.1016/j.snb.2010.03.083.
[19] C. de las H. Alarcón, S. Pennadam, C. Alexander, Stimuli responsive polymers for biomedical applications, Chem. Soc. Rev. 34 (2005) 276–285. http://dx.doi.org/10.1039/B406727D.
[20] E. Smela, Conjugated polymer actuators for biomedical applications, Adv. Mater. 15 (2003) 481–494. http://dx.doi.org/10.1002/adma.200390113.
[21] D. Morales, E. Palleau, M.D. Dickey, O.D. Velev, Electro-actuated hydrogel walkers with dual responsive legs, Soft Matter. 10 (2014) 1337–1348. http://dx.doi.org/10.1039/C3SM51921J.
[22] S. Kim, C. Laschi, B. Trimmer, Soft robotics: a bioinspired evolution in robotics, Trends Biotechnol. 31 (2013) 287–294. http://dx.doi.org/10.1016/j.tibtech.2013.03.002.
[23] G.H. Kwon, J.Y. Park, J.Y. Kim, M.L. Frisk, D.J. Beebe, S.-H. Lee, Biomimetic soft multifunctional miniature aquabots, Small 4 (2008) 2148–2153. http://dx.doi.org/10.1002/smll.200800315.
[24] K. Ueno, K. Matsubara, M. Watanabe, Y. Takeoka, An electro- and thermochromic hydrogel as a full-color indicator, Adv. Mater. 19 (2007) 2807–2812. http://dx.doi.org/10.1002/adma.200700159.
[25] L. Dong, A.K. Agarwal, D.J. Beebe, H. Jiang, Adaptive liquid microlenses activated by stimuli-responsive hydrogels, Nature 442 (2006) 551–554. http://dx.doi.org/10.1038/nature05024.
[26] G. Stoychev, L. Guiducci, S. Turcaud, J.W.C. Dunlop, L. Ionov, Hole-programmed superfast multistep folding of hydrogel bilayers, Adv. Funct. Mater. 26 (2016) 7733–7739. http://dx.doi.org/10.1002/adfm.201602394.
[27] J.L. Silverberg, J.-H. Na, A.A. Evans, B. Liu, T.C. Hull, C.D. Santangelo, R.J. Lang, R.C. Hayward, I. Cohen, Origami structures with a critical transition to bistability arising from hidden degrees of freedom 14 (2015) 389–393. http://dx.doi.org/10.1038/nmat4232.

[28] H. Thérien-Aubin, Z.L. Wu, Z. Nie, E. Kumacheva, Multiple shape transformations of composite hydrogel sheets 135 (2013) 4834–4839. http://dx.doi.org/10.1021/ja400518c.

[29] X. He, M. Aizenberg, O. Kuksenok, L.D. Zarzar, A. Shastri, A.C. Balazs, J. Aizenberg, Synthetic homeostatic materials with chemo-mechano-chemical self-regulation 487 (2012) 214–218. http://dx.doi.org/10.1038/nature11223.

[30] A. Sidorenko, T. Krupenkin, J. Aizenberg, Controlled switching of the wetting behavior of biomimetic surfaces with hydrogel-supported nanostructures, J. Mater. Chem. 18 (2008) 3841. http://dx.doi.org/10.1039/b805433a.

[31] S. Reddy, E. Arzt, A. del Campo, Bioinspired surfaces with switchable adhesion, Adv. Mater. 19 (2007) 3833–3837. http://dx.doi.org/10.1002/adma.200700733.

[32] Q. Zhao, X. Yang, C. Ma, D. Chen, H. Bai, T. Li, W. Yang, T. Xie, A bioinspired reversible snapping hydrogel assembly, Mater Horiz. 3 (2016) 422–428. http://dx.doi.org/10.1039/C6MH00167J.

[33] Z.L. Wu, M. Moshe, J. Greener, H. Therien-Aubin, Z. Nie, E. Sharon, E. Kumacheva, Three-dimensional shape transformations of hydrogel sheets induced by small-scale modulation of internal stresses, Nature Commun. 4 (2013) 1586. http://dx.doi.org/10.1038/ncomms2549.

[34] G. Stoychev, S. Zakharchenko, S. Turcaud, J.W.C. Dunlop, L. Ionov, Shape-programmed folding of stimuli-responsive polymer bilayers 6 (2012) 3925–3934. http://dx.doi.org/10.1021/nn300079f.

[35] J. Kim, J.A. Hanna, R.C. Hayward, C.D. Santangelo, Thermally responsive rolling of thin gel strips with discrete variations in swelling 8 (2012) 2375. http://dx.doi.org/10.1039/c2sm06681e.

[36] G. Stoychev, N. Puretskiy, L. Ionov, Self-folding all-polymer thermoresponsive microcapsules 7 (2011) 3277. http://dx.doi.org/10.1039/c1sm05109a.

[37] S. Zakharchenko, N. Puretskiy, G. Stoychev, M. Stamm, L. Ionov, Temperature controlled encapsulation and release using partially biodegradable thermo-magneto-sensitive self-rolling tubes 6 (2010) 2633. http://dx.doi.org/10.1039/c0sm00088d.

[38] A.K. Agarwal, L. Dong, D.J. Beebe, H. Jiang, Autonomously-triggered microfluidic cooling using thermo-responsive hydrogels, Lab. Chip. 7 (2007) 310. http://dx.doi.org/10.1039/b617767k.

[39] J. Wang, Z. Chen, M. Mauk, K.-S. Hong, M. Li, S. Yang, H.H. Bau, Self-actuated, thermo-responsive hydrogel valves for lab on a chip, Biomed. Microdev. 7 (2005) 313–322. http://dx.doi.org/10.1007/s10544-005-6073-z.

[40] T.S. Shim, S.-H. Kim, C.-J. Heo, H.C. Jeon, S.-M. Yang, Controlled origami folding of hydrogel bilayers with sustained reversibility for robust microcarriers, Angew. Chem. Int. Ed. 51 (2012) 1420–1423. http://dx.doi.org/10.1002/anie.201106723.

[41] K. Kumar, V. Luchnikov, B. Nandan, V. Senkovskyy, M. Stamm, Formation of self-rolled polymer microtubes studied by combinatorial approach 44 (2008) 4115–4121. http://dx.doi.org/10.1016/j.eurpolymj.2008.09.009.

[42] N. Bassik, B.T. Abebe, K.E. Laflin, D.H. Gracias, Photolithographically patterned smart hydrogel based bilayer actuators, Polymer 51 (2010) 6093–6098. http://dx.doi.org/10.1016/j.polymer.2010.10.035.

[43] S. Singamaneni, M.E. McConney, V.V. Tsukruk, Spontaneous self-folding in confined ultrathin polymer gels 22 (2010) 1263–1268. http://dx.doi.org/10.1002/adma.200903052.

[44] E. Wang, M.S. Desai, S.-W. Lee, Light-controlled Graphene–Elastin composite hydrogel actuators, Nano Lett. 13 (2013) 2826–2830. http://dx.doi.org/10.1021/nl401088b.

[45] K.E. Laflin, C.J. Morris, T. Muqeem, D.H. Gracias, Laser triggered sequential folding of microstructures, Appl. Phys. Lett. 101 (2012) 131901. http://dx.doi.org/10.1063/1.4754607.

[46] X. Zhang, C.L. Pint, M.H. Lee, B.E. Schubert, A. Jamshidi, K. Takei, H. Ko, A. Gillies, R. Bardhan, J.J. Urban, M. Wu, R. Fearing, A. Javey, Optically- and thermally-responsive programmable materials based on carbon nanotube-hydrogel polymer composites 11 (2011) 3239–3244. http://dx.doi.org/10.1021/nl201503e.

[47] N. Bassik, A. Brafman, A.M. Zarafshar, M. Jamal, D. Luvsanjav, F.M. Selaru, D.H. Gracias, Enzymatically triggered actuation of miniaturized tools, J. Am. Chem. Soc. 132 (2010) 16314–16317. http://dx.doi.org/10.1021/ja106218s.

[48] D.P. Holmes, M. Roché, T. Sinha, H.A. Stone, Bending and twisting of soft materials by non-homogenous swelling, Soft Matter. 7 (2011) 5188. http://dx.doi.org/10.1039/c0sm01492c.

[49] K.-U. Jeong, J.-H. Jang, D.-Y. Kim, C. Nah, J.H. Lee, M.-H. Lee, H.-J. Sun, C.-L. Wang, S.Z.D. Cheng, E.L. Thomas, Three-dimensional actuators transformed from the programmed two-dimensional structures via bending, twisting and folding mechanisms 21 (2011) 6824. http://dx.doi.org/10.1039/c0jm03631e.

[50] H.L. Lim, J.C. Chuang, T. Tran, A. Aung, G. Arya, S. Varghese, Dynamic electromechanical hydrogel matrices for stem cell culture, Adv. Funct. Mater. 21 (2011) 55–63. http://dx.doi.org/10.1002/adfm.201001519.

[51] M. Doi, M. Matsumoto, Y. Hirose, Deformation of ionic polymer gels by electric fields, Macromolecules 25 (1992) 5504–5511. http://dx.doi.org/10.1021/ma00046a058.

[52] S. Maeda, Y. Hara, R. Yoshida, S. Hashimoto, Active polymer gel actuators, Int. J. Mol. Sci. 11 (2010) 52–66. http://dx.doi.org/10.3390/ijms11010052.

[53] D. Suzuki, T. Kobayashi, R. Yoshida, T. Hirai, Soft actuators of organized self-oscillating microgels 8 (2012) 11447. http://dx.doi.org/10.1039/c2sm26477c.

[54] D. Eddington, Flow control with hydrogels 56 (2004) 199–210. http://dx.doi.org/10.1016/j.addr.2003.08.013.

[55] K.-F. Arndt, D. Kuckling, A. Richter, Application of sensitive hydrogels in flow control, Polym. Adv. Technol. 11 (2000) 496–505. http://dx.doi.org/10.1002/1099-1581(200008/12)11:8/12<496::AID-PAT996>3.0.CO;2-7.

[56] D. Morales, I. Podolsky, R. Mailen, T. Shay, M. Dickey, O. Velev, Ionoprinted multi-responsive hydrogel actuators, Micromachines 7 (2016) 98. http://dx.doi.org/10.3390/mi7060098.

[57] J. Kim, J.A. Hanna, M. Byun, C.D. Santangelo, R.C. Hayward, Designing responsive buckled surfaces by halftone gel lithography, Science 335 (2012) 1201–1205. http://dx.doi.org/10.1126/science.1215309.

[58] H. Lee, C. Xia, N.X. Fang, First jump of microgel; actuation speed enhancement by elastic instability, Soft Matter. 6 (2010) 4342. http://dx.doi.org/10.1039/c0sm00092b.

[59] S.V. Nikolov, P.D. Yeh, A. Alexeev, Self-propelled microswimmer actuated by stimuli-sensitive bilayered hydrogel, ACS Macro Lett. 4 (2015) 84–88. http://dx.doi.org/10.1021/mz5007014.

[60] B. Xu, H. Jiang, H. Li, G. Zhang, Q. Zhang, High strength nanocomposite hydrogel bilayer with bidirectional bending and shape switching behaviors for soft actuators, RSC Adv. 5 (2015) 13167–13170. http://dx.doi.org/10.1039/C4RA14545C.

[61] T.-A. Asoh, E. Kawamura, A. Kikuchi, Stabilization of electrophoretically adhered gel-interfaces to construct multi-layered hydrogels 3 (2013) 7947. http://dx.doi.org/10.1039/c3ra40409a.

[62] H. Zhang, C. Bian, J.K. Jackson, F. Khademolhosseini, H.M. Burt, M. Chiao, Fabrication of robust hydrogel coatings on polydimethylsiloxane substrates using micropillar anchor structures with chemical surface modification, ACS Appl. Mater. Interfaces 6 (2014) 9126–9133. http://dx.doi.org/10.1021/am501167x.

[63] H. Yuk, T. Zhang, G.A. Parada, X. Liu, X. Zhao, Skin-inspired hydrogel–elastomer hybrids with robust interfaces and functional microstructures, Nature Commun. 7 (2016) 12028. http://dx.doi.org/10.1038/ncomms12028.

[64] H. Yuk, T. Zhang, S. Lin, G.A. Parada, X. Zhao, Tough bonding of hydrogels to diverse non-porous surfaces, Nature Mater. 15 (2015) 190–196. http://dx.doi.org/10.1038/nmat4463.

[65] Q. Liu, G. Nian, C. Yang, S. Qu, Z. Suo, Bonding dissimilar polymer networks in various manufacturing processes, Nature Commun. 9 (2018) 846. http://dx.doi.org/10.1038/s41467-018-03269-x.

[66] J.N. Lee, C. Park, G.M. Whitesides, Solvent compatibility of poly(dimethylsiloxane)-based microfluidic devices, Anal. Chem. 75 (2003) 6544–6554. http://dx.doi.org/10.1021/ac0346712.

[67] W. Hong, Z. Liu, Z. Suo, Inhomogeneous swelling of a gel in equilibrium with a solvent and mechanical load, Int. J. Solids Struct. 46 (2009) 3282–3289. http://dx.doi.org/10.1016/j.ijsolstr.2009.04.022.

[68] J. Zhang, X. Zhao, Z. Suo, H. Jiang, A finite element method for transient analysis of concurrent large deformation and mass transport in gels, J. Appl. Phys. 105 (2009) 093522. http://dx.doi.org/10.1063/1.3106628.

[69] W. Guo, M. Li, J. Zhou, Modeling programmable deformation of self-folding all-polymer structures with temperature-sensitive hydrogels 22 (2013) 115028. http://dx.doi.org/10.1088/0964-1726/22/11/115028.

[70] S. Timoshenko, Analysis of bi-metal thermostats, J. Opt. Soc. Amer. 11 (1925) 233. http://dx.doi.org/10.1364/JOSA.11.000233.

[71] T.S. Kelby, M. Wang, W.T.S. Huck, Controlled folding of 2D Au-polymer brush composites into 3D microstructures, Adv. Funct. Mater. 21 (2011) 652–657. http://dx.doi.org/10.1002/adfm.201001744.

[72] E. Palleau, D. Morales, M.D. Dickey, O.D. Velev, Reversible patterning and actuation of hydrogels by electrically assisted ionoprinting 4 (2013). http://dx.doi.org/10.1038/ncomms3257.

[73] M. Christophersen, B. Shapiro, E. Smela, Characterization and modeling of PPy bilayer microactuators, Sensors Actuators B 115 (2006) 596–609. http://dx.doi.org/10.1016/j.snb.2005.10.023.

SUPPORTING INFORMATION

Stimuli-induced bi-directional hydrogel unimorph actuators

Shanliangzi Liu[‡], Elisa Boatti[†], Katia Bertoldi[†¶], and Rebecca Kramer-Bottiglio[‡*]*

[‡]School of Mechanical Engineering, Purdue University, West Lafayette, IN 47907, USA
[†]John A. Paulson School of Engineering and Applied Sciences, Harvard University, Cambridge, MA 02138, USA
¶Kavli Institute, Harvard University, Cambridge, MA 02138, USA

FIGURES

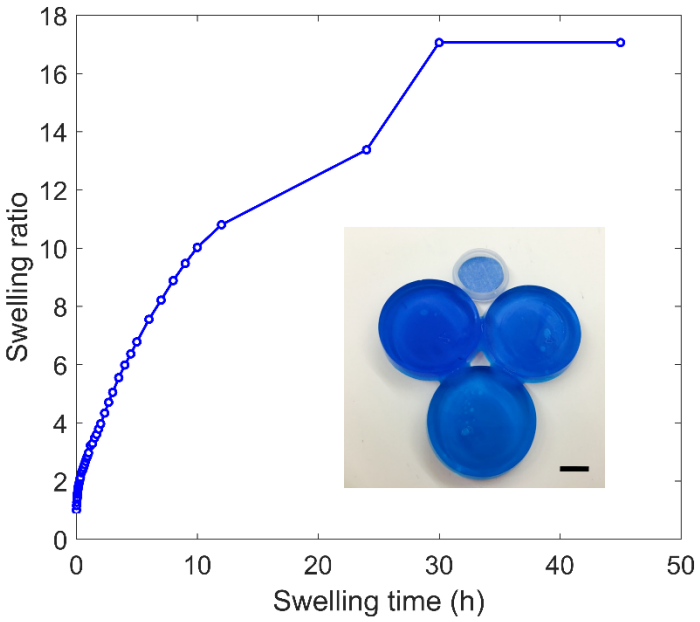

Figure S1. Plot of PAAm hydrogel swelling time as a function of swelling ratio. A PAAm hydrogel sample from a plastic cap was fully dried after photopolymerization and immersed in a water bath at room temperature. The sample was removed at regular time intervals, quickly weighed on a balance and then put back into the water bath. The swelling ratio is the ratio of the sample weight after each time interval to the initial weight of the fully dried sample. The swelling ratio is 17. The scale bar represents 10 mm.

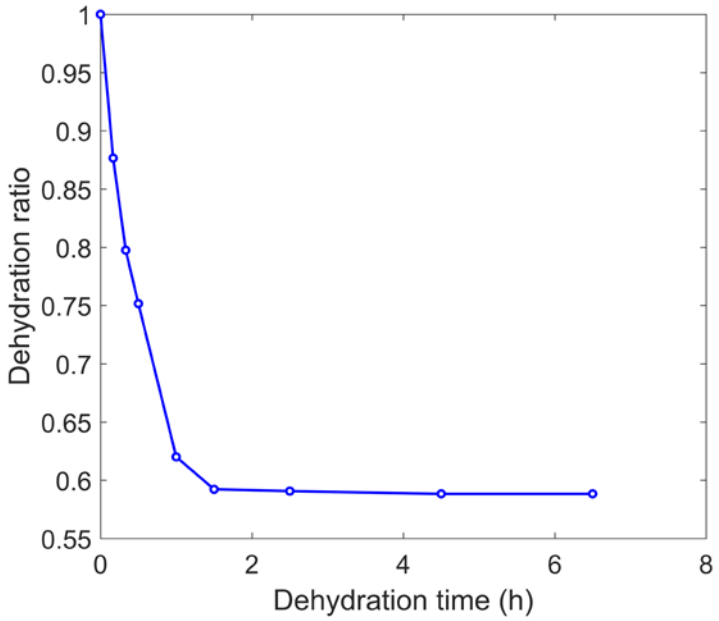

Figure S2. Plot of hydrogel-elastomer bilayer dehydration time as a function of dehydration ratio. The dehydration ratio is the ratio of dry weight after each time interval to the swollen weight of the sample right after photopolymerization.

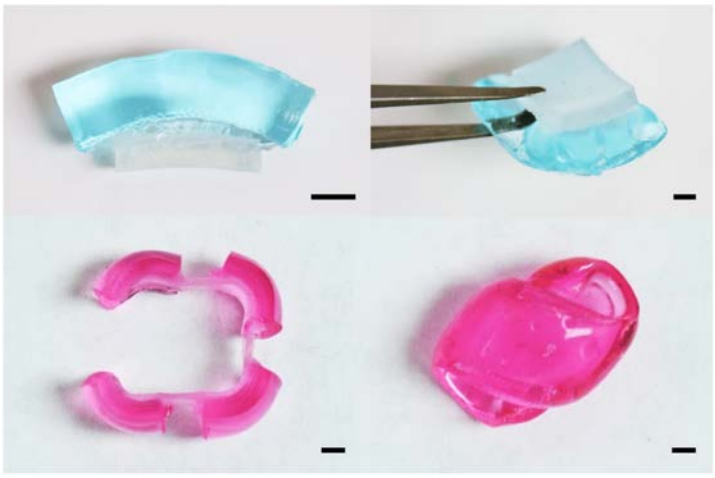

Figure S3. Images of hydrogel-elastomer bilayer structures in the swollen state. The hydrogel layer (in color) was bonded to an elastomer layer using the method reported in the Experimental Section and swelled in a water bath for a few hours. No delamination was observed when stretching, bending, twisting or squeezing the samples as shown in Video S1. The scale bars represent 3 mm.

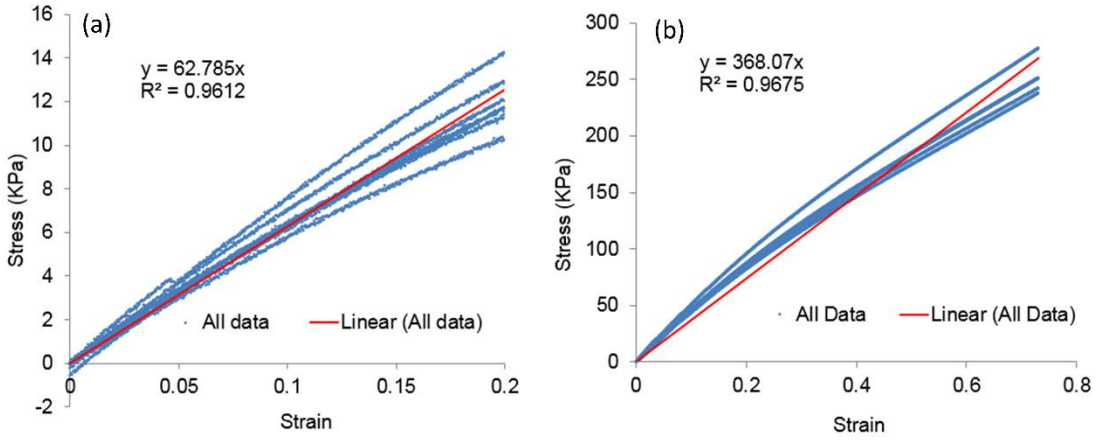

Figure S4. Tensile test results of PAAm hydrogel and PDMS elastomer. (a) PAAm stress-strain curves and a linear fit. (b) PDMS stress-strain curves and a linear fit. Young's moduli were derived by fitting the curves from linear regression. The Young's modulus of PDMS is E_{PDMS} = 0.368 MPa, polyacrylamide hydrogel is E_{PAAm} = 0.0628 MPa.

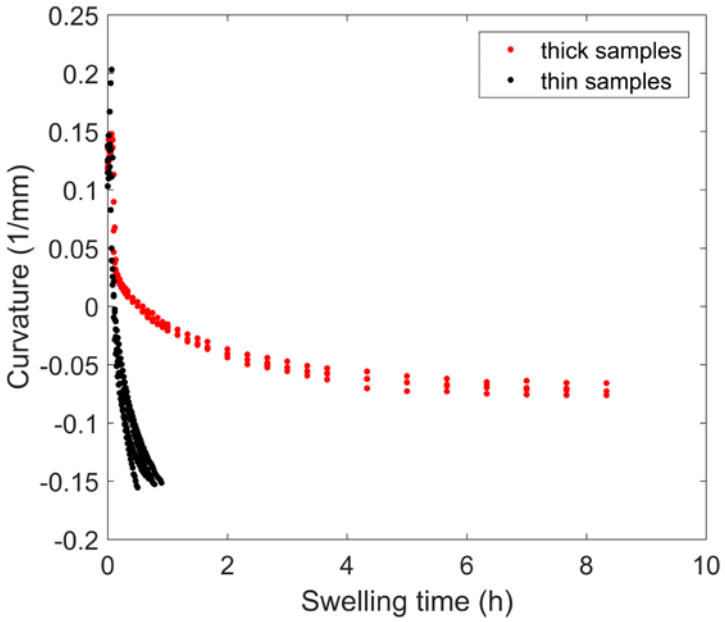

Figure S5. Additional experimental results of bending curvature evolution of hydrogel unimorph actuators in an aqueous environment. Both a thick and a thin unimorph sample were hydrated and dehydrated over four cycles using the setup described in the Experimental Section. The thicknesses of the hydrogel layers for both the thick and the thin sample are ~200 µm in the flat state. The thicknesses of the elastomer layers for the thick and the thin sample are ~1000 µm and ~600 µm, respectively.

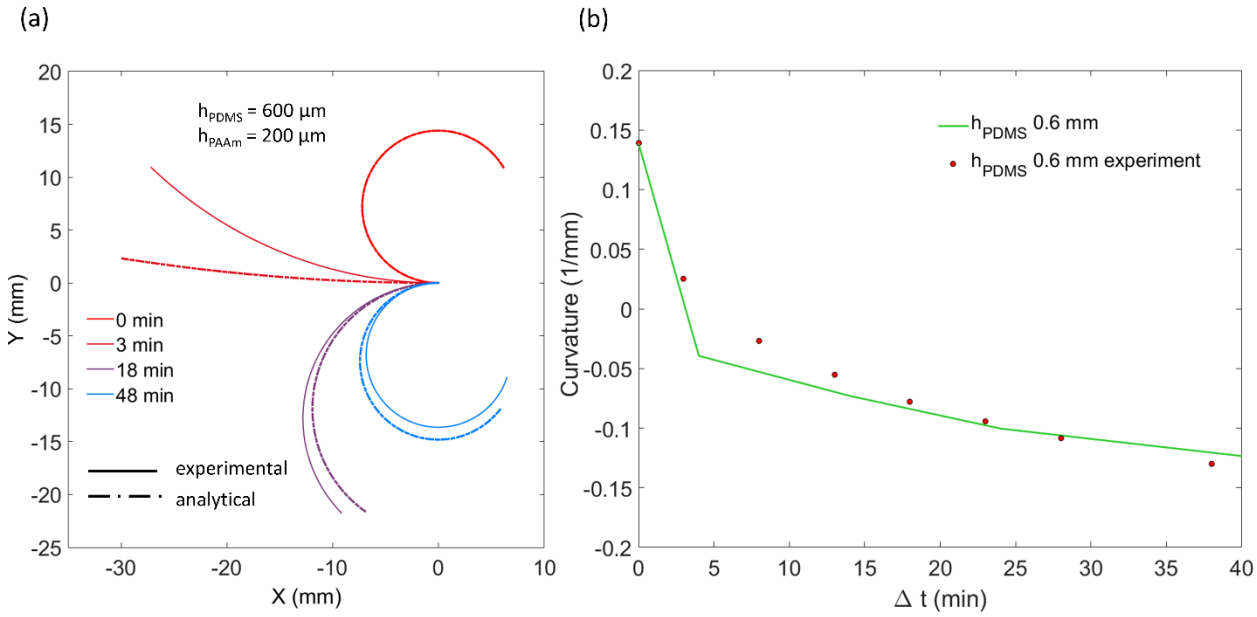

Figure S6. Additional analytical prediction of a hydrogel unimorph sample with h_{PDMS} = 600 µm. (a) Comparison between experimentally observed and analytically predicted configurations for a bistrip with h_{PDMS} = 600 µm and h_{PAAm} = 200 µm at different time instants. (b) Predicted curvature evolution (continuous line) and the experimental data (markers) for the bistrip with h_{PDMS} = 600 µm and h_{PAAm} = 200 µm.

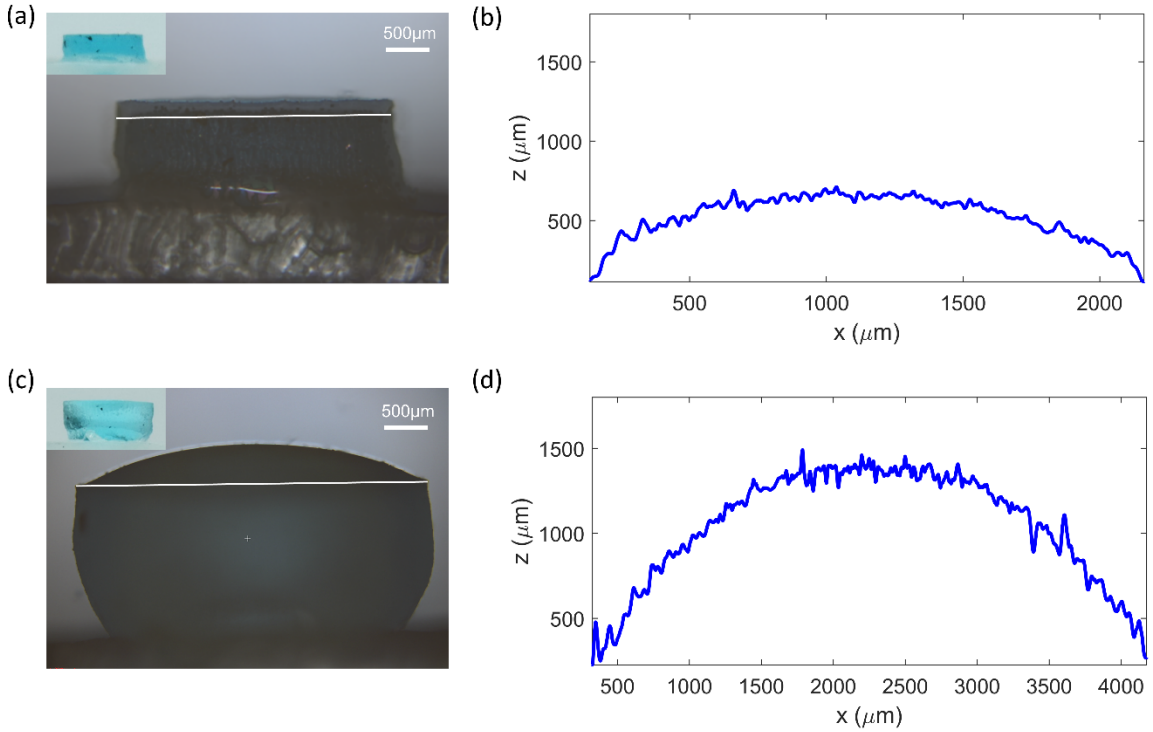

Figure S7. PAAm hydrogel pillars (in blue) bonded to a PDMS elastomer substrate in the (a) dehydrated and (c) hydrated state. Representative surface profiles are shown in (b,d).